Functional MRI of Uterine (Endometrial and Cervical) Cancer

35

Jennifer C. Wakefield, Kate Downey, and Nandita M. deSouza

Contents

Abbreviations

ADC	Apparent diffusion coefficient
AUC	Area under the curve
BOLD	Blood oxygen-level-dependent
CHESS	CHEmical-Shift Selective
CT	Computerized tomography
DCE	Dynamic contrast-enhanced
DWI	Diffusion-weighted imaging
DW-MRI	Diffusion-weighted MRI
ESN	Endometrial stromal nodule
ESS	Endometrial stromal sarcoma
EST	Endometrial stromal tumours
FIGO	International Federation of Gynecology and Obstetrics
FMPSPGR	Fast MultiPlanar Spoiled GRadient echo
ISW	Intrinsic susceptibility-weighted
IVIM	Intravoxel incoherent motion
MDA	Minimal deviation adenocarcinoma
MR	Magnetic resonance
MRI	Magnetic resonance imaging
MRS	Magnetic resonance spectroscopy
PRESS	Point-REsolved spectro scopy
STEAM	STimulated Echo Acquisition Mode
SWI	Susceptibility-weighted imaging
UES	Undifferentiated endometrial sarcoma
USPIO	Ultrasmall particles of iron oxide
VIBE	Volumetric interpolated breathhold examination
WHO	World Health Organization

J.C. Wakefield (✉) • K. Downey
N.M. deSouza, MD, FRCR
Department of Clinical Magnetic Resonance,
Institute of Cancer Research,
The Royal Marsden, Downs Road, Sutton, Surrey, SM2 5PT, UK
e-mail: jennie.wakefield@icr.ac.uk;
kate.downey@icr.ac.uk; nandita.desouza@icr.ac.uk

A. Luna et al. (eds.), *Functional Imaging in Oncology*,
DOI 10.1007/978-3-642-40582-2_12, © Springer-Verlag Berlin Heidelberg 2014

35.1 Introduction

Assessment of the presence and extent of gynaecological malignancy requires detailed anatomical information from the uterus, tubes and adnexa as well as coverage of the entire peritoneal cavity to assess peritoneal disease and visualisation of pelvic and abdominal lymph node stations. Computerised tomography (CT) has been, and in many instances, still is, the mainstay of imaging malignant gynaecological disease: it possesses advantages of speed and coverage with good spatial resolution (up to about 20 line pairs cm^{-1} on modern helical CT scanners) [1], and reformatting of axially acquired images in multiple planes is readily available on current software platforms. It is also sensitive to identifying fat or calcification within lesions, which are often crucial diagnostic indicators. However, the soft tissue contrast on CT is poor as it depends on tissue density which does not differ between tumour and surrounding normal tissue. This makes distinguishing tumour margins within structures such as cervix or endometrium difficult.

Magnetic resonance imaging (MRI) offers superior soft tissue differentiation because contrast is generated from differences in water relaxivity between tissues, which in turn depend on their cellular content, packing and matrix structure. Furthermore, it is possible to manipulate the contrast generated by appropriate programming of the RF pulse sequence to highlight relaxation properties in relation to the lattice (T1-W imaging), the neighbouring proton spins (T2-W imaging), the time course of shortening of T1 relaxation following injection of a weakly paramagnetic agent such as gadolinium (dynamic contrast-enhanced [DCE] imaging), the diffusion properties of primarily extracellular water (diffusion-weighted imaging [DWI]) and the magnetic susceptibility effects of deoxyhaemoglobin in hypoxic regions (R2* imaging/susceptibility-weighted imaging [SWI]) and to examine the presence of metabolites other than water (magnetic resonance spectroscopy [MRS]). Many examinations use a combination of these methods in a single multiparametric MRI protocol. It is important, however, to take account of the analysis of these multiple techniques which is intensive in time and expertise, tailoring the information acquired to answer the clinical question is essential.

35.2 Clinically Applied Techniques

35.2.1 Patient Preparation

Good patient preparation produces images of high diagnostic quality. As motion artefact from bowel peristalsis can significantly degrade image quality, administration of an antiperistaltic agent is routine in most oncology imaging centres with abdominopelvic MR imaging. Hyoscine butylbromide is readily available and safe to use. Glucagon is an alternative if the patient suffers from glaucoma or unstable angina. In our experience, intramuscular administration of the antiperistaltic agent into the patient's deltoid muscle immediately before their placement in the centre of the bore is the most effective method of administration, as absorption is relatively rapid and the duration of action is approximately 30 min, which is adequate for most gynaecological MRI examinations. The duration of action is too rapid with intravenous administration lasting only 10 min approximately, and it is difficult to predict the optimum time for imaging after oral administration as its absorption can be erratic [2].

Pelvic MRI image quality is optimal using a multichannel pelvic phased array coil, which enables coverage from the pelvic floor to the lower para-aortic nodal chains. A multichannel coil not only improves signal-to-noise ratio but also reduces scan time by allowing parallel imaging. If abdominal imaging is also to be performed, then the pelvic array coil needs to be repositioned, or a whole body multicoil arrangement can be used in newer scanners [2].

In dedicated MR imaging of the cervix, an endocavitary coil can be placed into the vagina to produce high spatial resolution images. This technique has proven particularly helpful for patient assessment prior to fertility-sparing surgery. These coils can be used in women with a cervix remaining and small tumours (stages IA and IB). There are two principal endocavitary coil types. The first is the balloon design, which has the advantage of self-immobilisation inside the vagina. In order to further reduce coil movement during the scan, it is best to place a sandbag over its handle. The second endocavitary coil type is a solenoid design that envelopes the

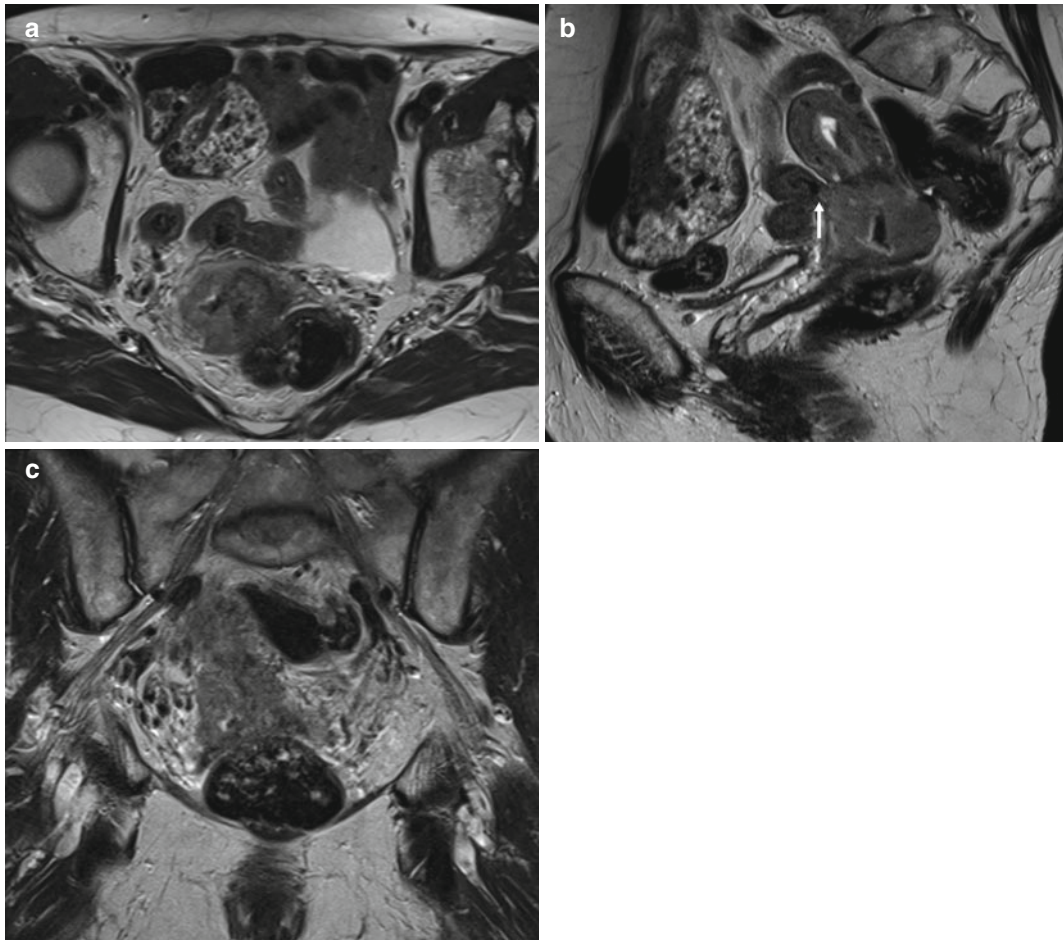

Fig. 35.1 Squamous cell carcinoma of the cervix in a 79-year-old female. T2-weighted transverse (**a**), sagittal (**b**), and coronal (**c**) images demonstrate a large cervical mass with irregular margins. Parametrial extension is seen bilaterally (**a**). Small bowel involvement is seen in **b** (*arrow*) indicating the utility of multiplanar orthogonal views

cervix. This coil has a signal-to-noise ratio advantage over the balloon coil, enabling improved delineation of smaller tumours and parametrial invasion, but it has to be immobilised using an external clamp to grasp the handle [2].

35.2.2 Imaging Sequences

35.2.2.1 Morphological MRI

T2-weighted imaging is the most important sequence for imaging of both cervical and endometrial cancers, as there is good contrast definition between the intermediate signal intensity tumour and the adjacent normal uterine or cervical tissue. It is helpful to perform T2-weighted images in three orthogonal planes through the uterine body or cervix. Additional axial T1-weighted images assist in the identification of blood and, in combination with the T2-weighted images, aid the assessment of the parametrium, parametrial lymph nodes, obturator vessels and direct invasion of the rectosigmoid colon and urinary bladder (Fig. 35.1).

35.2.2.2 Dynamic Contrast-Enhanced MRI (DCE)

This functional imaging technique gives an assessment of tumour vascularity. Consecutive, three-dimensional, fat-suppressed gradient echo images through the organ of interest are acquired rapidly

before, during and after a bolus injection of a paramagnetic contrast agent, such as gadolinium, that increases T1 signal intensity. The degree of enhancement in the early vascular phase is determined by blood flow, vascular density, capillary permeability and capillary surface area and in the interstitial phase by extravascular space volume. The pharmacokinetic profile of the injected contrast agent allows generation of quantitative parameters such as the transfer constant K^{trans} and extracellular extravascular leakage space v_e [3]. The DCE data can also be analysed semiquantitatively, producing parameters such as IAUGC (initial area under the gadolinium curve). The uterine tumour enhances poorly and the peak enhancement of the highly perfused myometrium occurs at 90 s post-contrast administration. Therefore, an optimum imaging time is between 60 and 90 s when contrast difference between the uterine tumour and the myometrium is maximal. Cervical mucosa starts to enhance at approximately 30 s post-contrast administration and peaks at approximately 120 s. The fibromuscular stroma of the cervix enhances more slowly [2].

35.2.2.3 Diffusion-Weighted Imaging (DWI)

Diffusion-weighted imaging (DWI) exploits the thermally driven motion of water molecules, which in biological tissue is modified by cell membrane integrity, extracellular microarchitecture, active transport mechanisms and microcirculation and detects molecular displacements at a cellular scale. No exogenous contrast agent is necessary because the image contrast is derived from the differences in the restriction of water movement between the tissues. Fat saturation is routinely applied to diffusion-weighted images. Alterations in the amplitude, duration and spacing of magnetic field gradients can incrementally sensitise DWI to diffusion. The diffusion weighting is determined by the b value, with values from 0 to 2,000 smm^{-2} currently used in clinical practice. At relatively low *b* values (<100–150 smm^{-2}), rapid signal loss occurs in structures where water motion is relatively free, for example, in fluid collections, flowing vessels or ducts. This phenomenon is termed intravoxel incoherent motion (IVIM) and gives a perfusional component to the diffusion data. The quantitative parameter apparent diffusion coefficient (ADC) is derived from the exponential attenuation of signal intensity between at least two *b* values. Restricted diffusion is indicated by bright foci on the high *b* value diffusion images, with a corresponding area of low signal on the ADC map (Fig. 35.2). It is important to compare the DWI with the corresponding morphological imaging to improve anatomical correlation, as DWI has low signal-to-noise ratio, resulting in poor spatial resolution (Fig. 35.2).

35.2.2.4 Intrinsic Susceptibility-Weighted (ISW) or Blood Oxygen-Level-Dependent (BOLD) MRI

Intrinsic susceptibility-weighted (ISW) or blood oxygen-level-dependent (BOLD) MRI images are typically a T2* gradient echo sequence. Deoxyhaemoglobin is paramagnetic and causes a slight increase in T2*. ISW/BOLD MRI uses this property to reflect the oxygenation status of tissue immediately adjacent to perfused microvessels. Unfortunately, T2* readings can also be affected by blood flow, pH, carbon dioxide tension and haematocrit. The BOLD effect can be quantified by plotting the natural log of signal intensity on the T2* sequence against the echo time to derive tissue relaxivity. The quantitative parameter, R2*, is derived from the power of the exponent (1/T2*). When the blood volume in the tissue of interest is known, these R2* maps reflect the local concentration of deoxyhaemoglobin. The change in signal intensity in ISW/BOLD is low, and therefore, the R2* gives an assessment of differential areas of oxygenation. The use of vasomodulation techniques with BOLD/ISW MRI, such as breathing carbogen (5 % CO_2, 95 % O_2) or 100 % oxygen, enables robust measurements or direct correlation with pO_2 values. These vasomodulation techniques augment the ISW/BOLD signal by increasing perfusion as a result of CO_2 vasodilatory effects and increased oxygenation. These

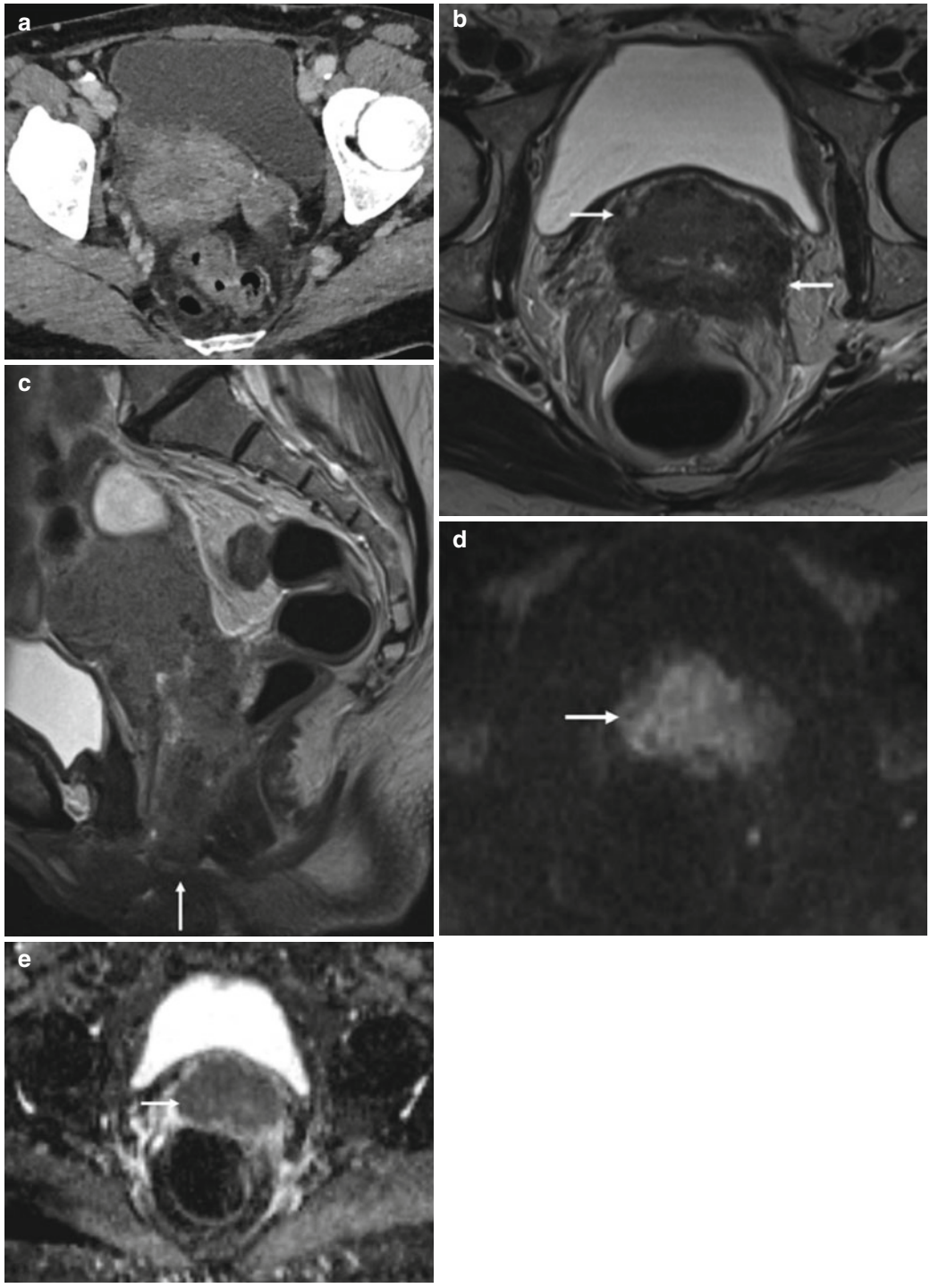

Fig. 35.2 Squamous cell carcinoma of the cervix in a 70-year-old female: transverse CT (**a**), T2-weighted transverse (**b**), and sagittal (**c**) images demonstrate a bulky mass centered on the cervix and extending into both parametria (**b**, *arrows*) and inferiorly to the vaginal introitus (**c**, *arrow*). Tumor involves the adjacent anterior rectal wall (**c**). The tumor (**d** and **e**, *arrow*) demonstrates impeded diffusion on the transverse DWI (**d**, **b** = 1,200 smm^{-2}) and corresponding ADC map (**e**, **b** = 50, 400, 800, 1,200 smm^{-2})

vasomodulation techniques are not well tolerated in human studies due to technical difficulties in gas delivery and patient distress. In a preliminary study by Hallac et al. [4], BOLD/ISW MRI at 3 T was feasible in cervical cancer with all 10 patients and 3 healthy volunteers tolerating the 100 % oxygen vasomodulation technique.

35.2.2.5 Proton Magnetic Resonance Spectroscopy (MRS)

Proton magnetic resonance spectroscopy (MRS) derives its signal from the different resonant frequencies of protons within a molecule due to magnetic diatomic interactions within the molecular structure. Data may be acquired from a single voxel of interest using Point-REsolved SpectroScopy (PRESS) or a STimulated Echo Acquisition Mode (STEAM). A CHEmical-Shift Selective (CHESS) pulse is commonly used for water suppression. The acquisition is fairly fast (1–3 min). Two-dimensional or three-dimensional chemical shift imaging obtains data from several voxels within a slab or volume of tissue by repetition of PRESS- or STEAM-type sequences to which spatial phase encoding has been added. Acquisition time relates to the number of phase-encoding steps and is in the order of 10–20 min. Resonant signals are displayed as a function of frequency (spectrum) after Fourier transform as a series of peaks on the chemical shift axis (expressed in parts per million, ppm), which are unique for different metabolites. The ppm scale describes the shift in hertz from a reference frequency divided by the excitation frequency of the external magnetic field. Although spectral resolution is improved at higher magnetic field strengths (3 T and above) due to the higher signal-to-noise ratio, inherent field inhomogeneities result in metabolites resonating at a range of frequencies; nevertheless, typical peak patterns can be recognised (choline 3.2 ppm, creatine 3.0 ppm, lactate 1.4 ppm). Absolute quantification in vivo is hampered by the absence of internal standards of concentration so relative concentrations are frequently used to characterise tumour and assess response.

Table 35.1 FIGO staging for carcinoma of the endometrium [5]

Stage I[a]	Tumour confined to the corpus uteri
IA[a]	No or less than half myometrial invasion
IB[a]	Invasion equal to or more than half of the myometrium
Stage II[a]	Tumour invades cervical stroma, but does not extend beyond the uterus[b]
Stage III[a]	Local and/or regional spread of the tumour
IIIA[a]	Tumour invades the serosa of the corpus uteri and/or adnexa[c]
IIIB[a]	Vaginal and/or parametrial involvement[c]
IIIC[a]	Metastases to pelvic and/or para-aortic lymph nodes[c]
IIIC1[a]	Positive pelvic nodes
IIIC2[a]	Positive para-aortic lymph nodes with or without positive pelvic lymph nodes
Stage IV[a]	Tumour invades bladder and/or bowel mucosa and/or distant metastases
IVA[a]	Tumour invasion of bladder and/or bowel mucosa
IVB[a]	Distant metastases, including intra-abdominal metastases and/or inguinal lymph nodes

[a]Either G1, G2 or G3 (*G* grade)
[b]Endocervical glandular involvement only should be considered as stage I and no longer as stage II
[c]Positive cytology has to be reported separately without changing the stage

35.3 Staging

35.3.1 Local Staging

35.3.1.1 Endometrium

Endometrium T2-W imaging in two or three planes orthogonal to the uterine body is the mainstay of detection and staging endometrial cancer. The revised International Federation of Gynecology and Obstetrics (FIGO) staging system is given in Table 35.1 [5]. The depth of myometrial invasion by endometrial carcinoma on preoperative imaging assessment is an important distinction as it strongly affects the incidence of metastasis to regional nodes and may therefore influence surgical strategies (Figs. 35.3 and 35.4).

MRI using a T2-W sequence best demonstrates disruption of normal myometrial zonal differentiation. In the postmenopausal patient, uterine involution and reduction of zonal

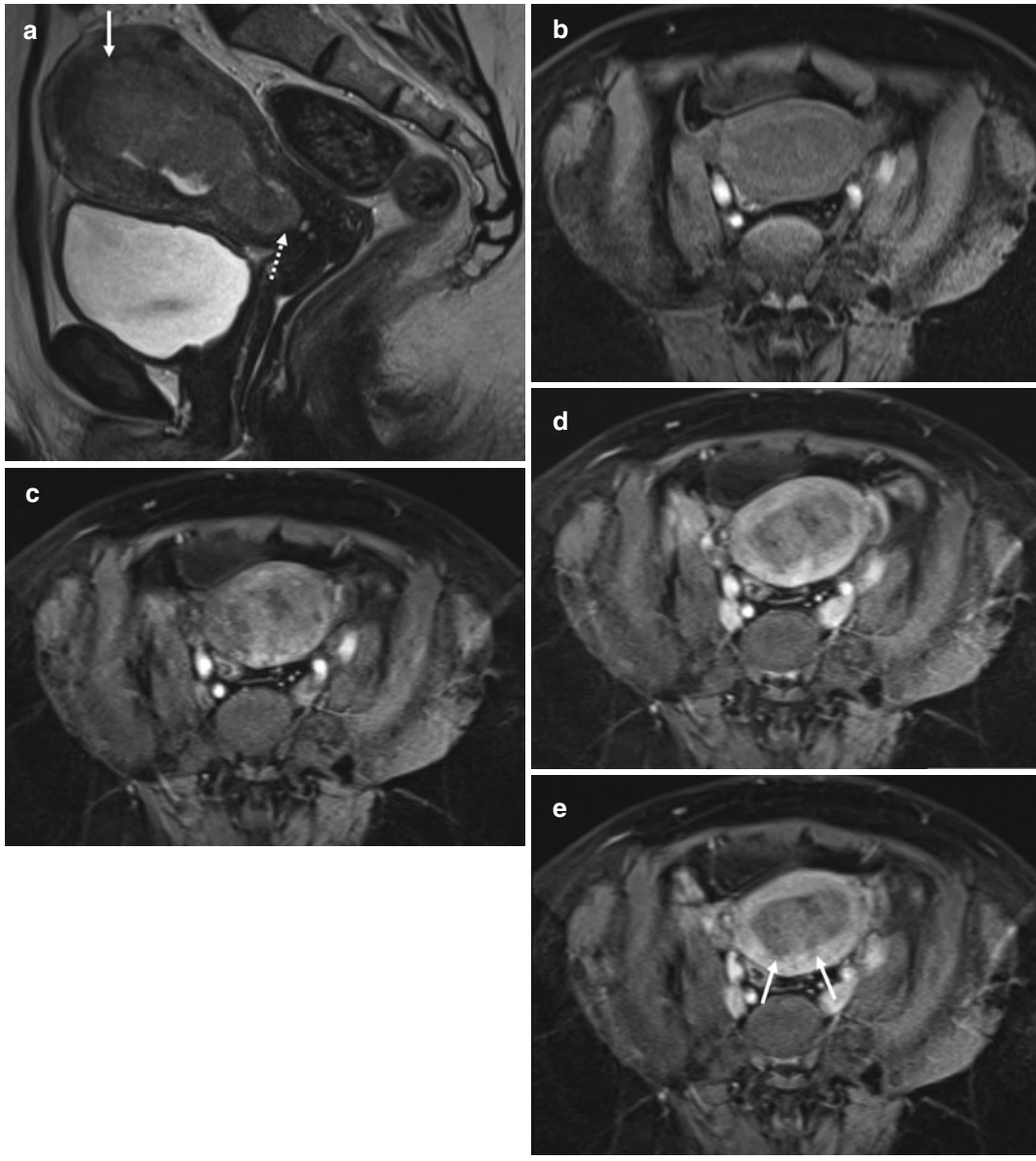

Fig. 35.3 Endometrial cancer in a 58-year-old female: sagittal T2-weighted image (**a**) demonstrates a large intermediate signal endometrial mass with myometrial invasion superiorly (*arrow*) and cervical stromal involvement at the internal os (*dotted arrow*). The normal myometrium shows progressive enhancement on the axial T1-weighted volumetric interpolated breathhold examination (VIBE) fat saturated series; [pre- (**b**), immediate (**c**), 1 min (**d**), and 2 min (**e**) post- gadolinium], compared to the endometrial tumor, which enhances poorly. The contrast between tumor and myometrium is maximal at 2 min post-gadolinium, making the myometrial invasion identifiable as superficial only (<50 % myometrial involvement) (*arrows*, **e**)

differentiation make it more difficult to assess myometrial infiltration. Some early studies advocated the addition of contrast enhancement because of a higher demonstrable accuracy for delineating the tumour than endovaginal ultrasound or CT [6, 7], although more recently this has been superseded by higher resolution T2-weighted imaging as a result of improvements in scanner hardware and software. MRI at 3 T does not offer significant benefit over

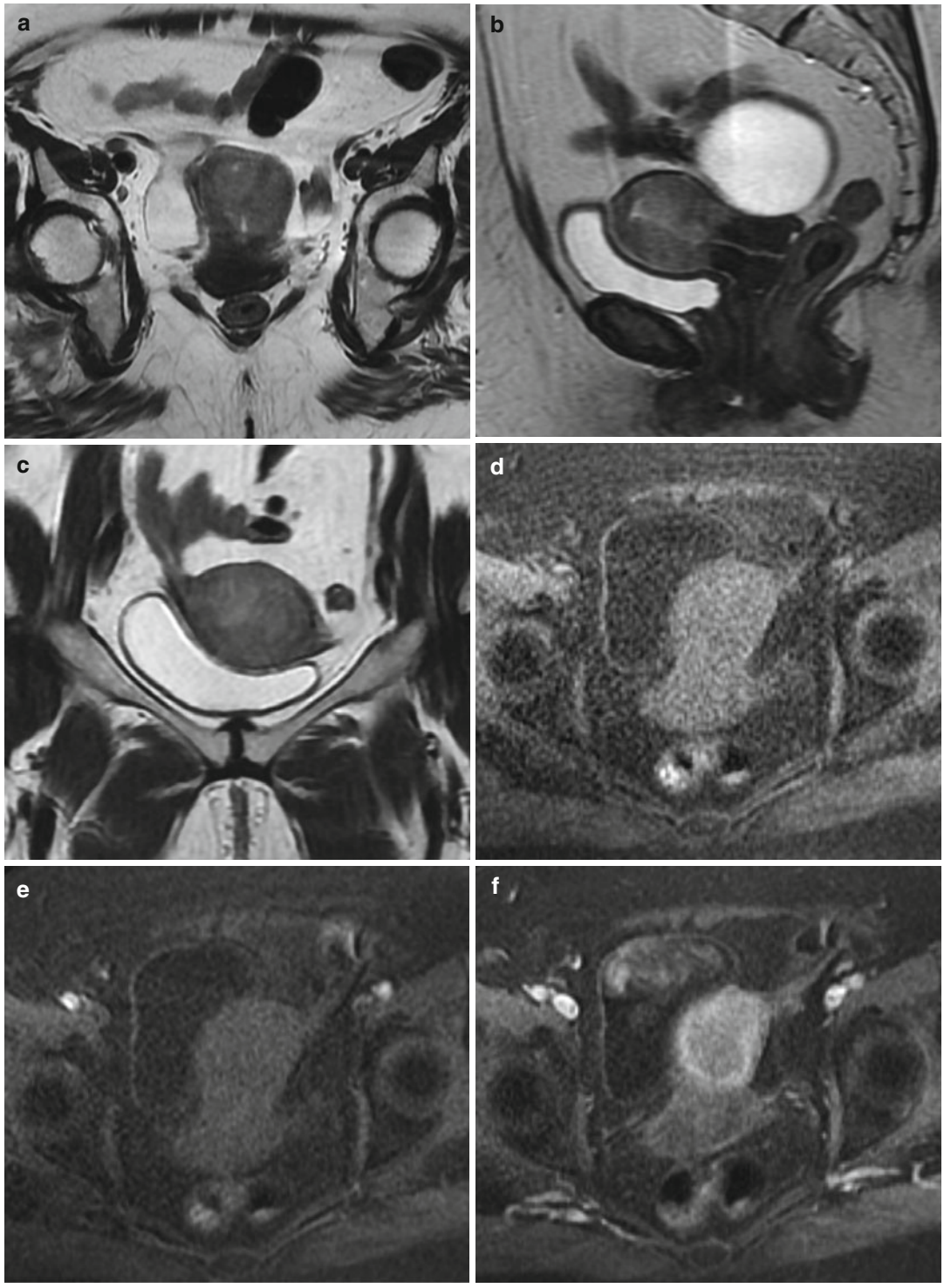

Fig. 35.4 Endometrioid adenocarcinoma of the endometrium in a 80-year-old female. T2-weighted transverse (**a**), sagittal (**b**), and coronal (**c**) demonstrate abnormal intermediate signal intensity affecting the uterine corpus, in keeping with a diffuse infiltrative tumor. Transverse T1-weighted VIBE fat saturated images [pre- (**d**), immediate (**e**), 1 min (**f**), and 2 min post- gadolinium (**g**)] demonstrate a poorly enhancing endometrial tumor with deep myometrial invasion (*arrow*)

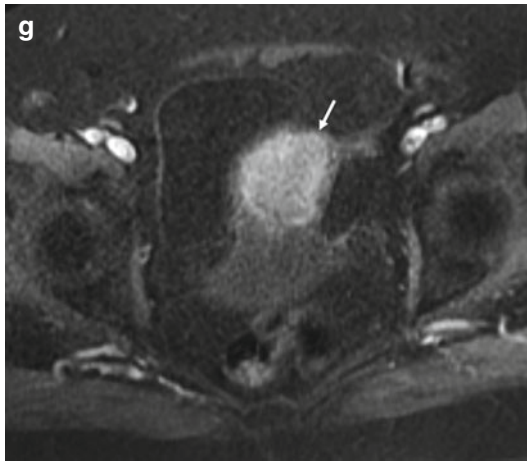

Fig. 35.4 (continued)

1.5 T, although faster imaging protocols may be helpful in uncooperative patients.

Gadolinium-enhanced dynamic sequences increase the accuracy of MR imaging in diagnosing the depth of myometrial invasion (Figs. 35.3 and 35.4). In particular, they improve the visualisation of the inner myometrium, the so-called subendometrial enhancing zone, whose disruption or changes are essential for diagnosing myometrial invasion. The major diagnostic advantage of these enhanced techniques is in postmenopausal women, where visualisation of the junctional zone may be difficult on the T2-W sequences. In postmenopausal women, the accuracy in estimating myometrial invasion with T2-W images, contrast-enhanced T1-weighted images and dynamic contrast-enhanced MRI was 66.7, 77.8 and 92.6 %, respectively [8]. In a more recent study of 45 women, Nasi et al. [9] showed that gadolinium enhancement with Fast MultiPlanar Spoiled GRadient echo (FMPSPGR) had a global sensitivity and specificity of 90.6 and 93.3 %, respectively, with a mean negative predictive value of 96.3 % and a mean positive predictive value of 88 % compared to the FSE T2-W sequence (global sensitivity and specificity of 80.6 and 87.6 %, respectively, mean negative predictive value 92.6 %, mean positive predictive value 86 %) giving contrast-enhanced sequences a higher staging accuracy (95 % vs.78 %).

Although DCE is routinely used for staging endometrial cancer and is highly accurate, DWI also can be useful in determining the depth of myometrial invasion. It can be particularly helpful in tumours that are either iso- or hyperintense relative to the myometrium on T2-W images or when the use of intravenous contrast medium is contraindicated. Recently, in a prospective study, Rechichi et al. 2010 [10] suggested that the accuracy of DW MRI in assessing myometrial invasion was comparable to DCE MRI which it could replace in preoperative evaluation.

DWI is also useful in detecting the presence of endometrial cancer. On DW images, endometrial cancer demonstrates high signal intensity with corresponding low signal intensity on ADC maps: the quantified ADC values were discriminatory between benign and malignant endometrial lesions [11]. The mean ± SD ADC of stage IA endometrial carcinoma has been reported as $0.878 \pm 0.185 \times 10^{-3}$ mm²/s, which was significantly lower ($P < 0.01$) than that of normal endometrium ($1.446 \pm 0.246 \times 10^{-3}$ mm²/s) and benign endometrial lesions ($1.637 \pm 0.178 \times 10^{-3}$ mm²/s) without any overlap [12]. In a study of 25 patients, sensitivity, specificity and accuracy for detecting tumour were 84.6, 100 and 92 %, respectively [13]. However, one should be aware that there is no reliable cut-off ADC value that is diagnostic of presence of malignancy. DWI can also be helpful in cases where the endometrial biopsy is technically impossible, the histopathology results are inconclusive or when the MRI is performed for different clinical indications, such as evaluation of an indeterminate adnexal lesion, and the endometrial abnormality is an incidental finding.

High-grade endometrial carcinomas have high cellular density and may be expected to have lower ADC values compared to low-grade tumours. However, ADC values do not correlate with histological tumour grade, the depth of myometrial invasion or whether lymph node metastases are present [14]. The hope that DWI may influence surgical planning by improving preoperative detection of high-grade tumours therefore is not a clinical reality; this may in part be due to the tumour necrosis associated with poorly differentiated tumours that can increase ADC values.

DW MRI can be also useful in incidental detection of drop metastases within the cervix or metastatic foci outside the uterus, such as adnexa or peritoneum [15].

35.3.1.2 Cervix

The primary tumour is best assessed using T_2-weighted MR imaging which is superior to CT in detection (sensitivity 75 % vs. 51 %, $p<0.005$) and in staging (accuracy 75–77 % vs. 32–69 %, $p<0.025$) [16, 17]. The revised FIGO staging is given in Table 35.2 [5]. The soft tissue contrast of MR imaging differentiates intermediate signal intensity tumour from low signal intensity stroma and identifies the presence and extent of the tumour in three planes orthogonal to the cervix. The coronal and axial planes are used for determining direct extension into the parametrium, the axial plane for determining extension into the bladder and rectum and the sagittal plane for determining extension into the uterine body, bladder and rectum [18]. Fast spin-echo T2-W images provide the best image contrast. Measuring tumour volume on MRI is of paramount importance, the size of tumour burden is a stronger predictor of outcome than invasion beyond the anatomical margins of the uterus [19], and it also gives an indication of likely lymph node involvement [20]. MRI has been found to be accurate in assessing cervical tumour dimensions to within 0.5 cm [21–26], and tumour volume at MRI compared to histology has shown good correlation (up to 0.98) [21, 27–30], but MRI volumes correlate only weakly with clinical stage [31].

Dynamic contrast enhancement was first advocated over a decade and a half ago for evaluating cervical cancer. Over this time, perfusion studies have largely focused on evaluating sensitivity and specificity of stromal invasion. In a correlative study, DCE gave a higher sensitivity and specificity for diagnosing stromal invasion >3 mm than standard T2-weighted imaging (accuracy 98 % vs. 76 %) [32]. Contrast enhancement has been used for assessment of tumour angiogenesis [33] and vascular density has been associated with low pO_2 in preliminary validation studies in cervical cancer [34] with a positive correlation observed between level of contrast enhancement on DCE and pO_2 measured by oximetry [35]. However, there is no diagnostic advantage of

Table 35.2 FIGO staging for carcinoma of the cervix uteri [5]

Stage I	The carcinoma is strictly confined to the cervix (extension to the corpus would be disregarded)
IA	Invasive carcinoma, which can be diagnosed only by microscopy, with deepest invasion ≤5 mm and largest extension ≤7 mm
IA1	Measured stromal invasion of ≤3.0 mm in depth and extension of ≤7.0 mm
IA2	Measured stromal invasion of >3.0 mm and not >5.0 mm with an extension of not >7.0 mm
IB	Clinically visible lesions limited to the cervix uteri or preclinical cancers greater than stage IA[a]
IB1	Clinically visible lesion ≤4.0 cm in greatest dimension
IB2	Clinically visible lesion >4.0 cm in greatest dimension
Stage II	Cervical carcinoma invades beyond the uterus but not to the pelvic wall or to the lower third of the vagina
IIA	Without parametrial invasion
IIA1	Clinically visible lesion ≤4.0 cm in greatest dimension
IIA2	Clinically visible lesion >4.0 cm in greatest dimension
IIB	With obvious parametrial invasion
Stage III	The tumour extends to the pelvic wall and/or involves lower third of the vagina and/or causes hydronephrosis or nonfunctioning kidney[b]
IIIA	Tumour involves lower third of the vagina with no extension to the pelvic wall
IIIB	Extension to the pelvic wall and/or hydronephrosis or nonfunctioning kidney
Stage IV	The carcinoma has extended beyond the true pelvis or has involved (biopsy proven) the mucosa of the bladder or rectum. A bullous oedema, as such, does not permit a case to be allotted to stage IV
IVA	Spread of the growth to adjacent organs
IVB	Spread to distant organs

[a]All macroscopically visible lesions—even with superficial invasion—are allotted to stage IB carcinomas. Invasion is limited to a measured stromal invasion with a maximal depth of 5.00 mm and a horizontal extension of not >7.00 mm. Depth of invasion should not be >5.00 mm taken from the base of the epithelium of the original tissue—superficial or glandular. The depth of invasion should always be reported in mm, even in those cases with 'early (minimal) stromal invasion' (~1 mm). The involvement of vascular/lymphatic spaces should not change the stage allotment

[b]On rectal examination, there is no cancer-free space between the tumour and the pelvic wall. All cases with hydronephrosis or nonfunctioning kidney are included, unless they are known to be due to another cause

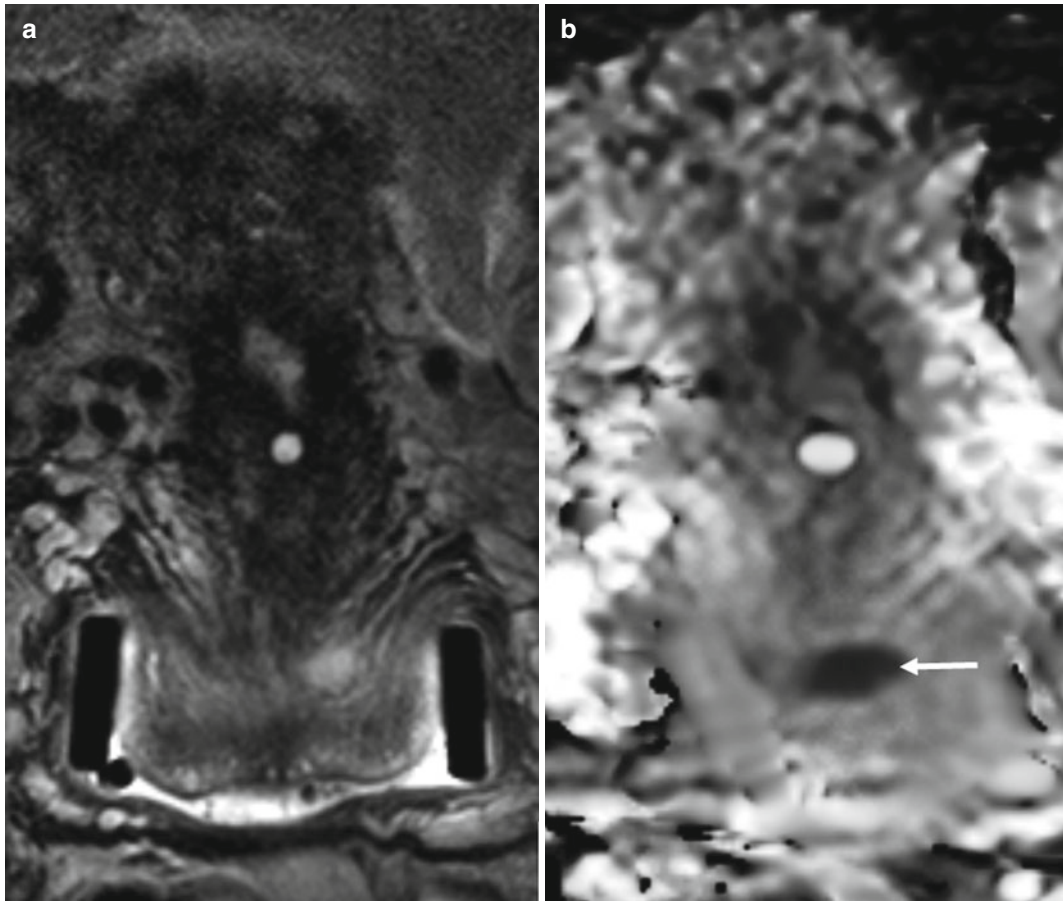

Fig. 35.5 Squamous cell carcinoma of the cervix in a 26-year-old female who is being considered for fertility sparing surgery. Endovaginal coronal T2-weighted image (**a**) demonstrates a large LLETZ defect with a small and ill-defined area of intermediate signal in the roof of this defect. This represents a small cervical tumor, which is better appreciated on the corresponding ADC map (**b**), (**b**=0,100, 300, 500, 800 smm^{-2}) as a focal area of low signal (*arrow*)

DCE over T2-W imaging in staging cervical cancer and no correlation with tumour aggressiveness [36] so that these images are not routinely used.

With the introduction of screening, the emphasis has shifted towards detecting early-stage disease. In these patients with clinical IA and IB1 cervical cancer referred following cone biopsy on which invasive disease is an unexpected finding, identifying disease within the cervix is difficult on T2-W imaging because it is of small volume. Also, patients are often referred following positive cone biopsies when most or all of the invasive disease has been removed. Image resolution with external phased array coils is limited with small-volume disease and can be significantly improved by the use of receiver coils close to the region of interest as they provide significant increases in signal-to-noise ratio. An endovaginal technique is well tolerated and has been shown to be accurate in the detection and location of cervical cancers and exclusion of early parametrial extension [27, 37–39] and has been found to be more sensitive than external coil techniques in the detection of small-volume disease. Because local oedema and granulation tissue make distinction between residual tumour and post-operative change difficult with an endovaginal technique using T2-weighted images, DWI sequences have been implemented to differentiate small tumours from postsurgical change based on water diffusion within tissues (Fig. 35.5). An improved sensitivity for tumour detection has been found

when DWI is used in conjunction with T2-W MRI in these cases with good interobserver agreement [40].

Malignant cervical tissue demonstrates restricted diffusion and hence reduced ADC values when compared to normal tissue. High b value (>800 s/mm^2) DWI and ADC maps allow differentiation of benign from malignant zones of cervix with high sensitivity and specificity [41–45]. Preliminary data also demonstrates the ability of ADC to differentiate histological type and grade of tumour [44, 46]. In a prospective study, ADC values were statistically significantly lower in malignant compared to benign cervical tissue (1.1×10^{-3} mm^2/s vs. 1.7×10^{-3} mm^2/s, $P<0.001$) and poorly differentiated compared to well-differentiated tumours (1.1×10^{-3} mm^2/s vs. 1.2×10^{-3} mm^2/s, $P=0.01$) [44]. However, there was no significant difference when tumours were divided by other histological features (type, lymphovascular invasion and lymph node metastasis). More recently, an increasing literature suggests ADC of squamous carcinomas to be lower than adenocarcinomas [46, 47] but needs quantification rather than visualisation alone for evaluation of these differences.

CT and MRI have both been used to assess parametrial spread: both result in false-positive diagnoses [24, 48] likely from misinterpreting inflammatory parametrial soft tissue strands associated with tumour as actual tumour invasion. DCE is superior to conventional T2-W images and T1-W post-contrast images in detecting the presence of parametrial extension by distinguishing tumour from normal cervical stroma and myometrium [49].

There is no evidence for the benefit of MRS in diagnosis of cervical cancer. In the proton spectrum, changes have largely been reported in the lipid and choline fractions. A doubling of lipids on ex vivo spectroscopy in malignant cervical tissue compared with benign cervical tissue has been reported [50] although there was no correlation with tumour load. Choline observed in vivo in cervical cancer was not significantly different from that reported in benign lesions [51] so that this technique is not yet clinically useful.

35.3.2 Nodal Staging and Distant Spread

The assessment of lymph node status with functional MRI techniques remains poor. In a study of 37 patients with endometrial cancer, sensitivity, specificity, diagnostic accuracy and positive and negative predictive values for lymph node assessment on contrast-enhanced MRI were 50, 95, 90, 50 and 95 %, respectively [52], so that recognition of abnormal lymph nodes is still dependent on size criteria. This prompted endeavour on developing extrinsic contrast agents for detecting metastatic nodes. Over the last decade, there has been significant research activity around production of a lymph node-specific MR contrast agent to allow the identification of malignant nodal infiltration independent of the lymph node size. This novel MR contrast agent is a nanoparticle (mean diameter, 30 nm) and is composed of an iron oxide core, coated with low molecular weight dextran (ultrasmall particles of iron oxide, USPIO). The particles, administered intravenously, are taken up by macrophages in the reticuloendothelial system, predominantly within the lymph nodes. Their uptake results in marked loss of signal intensity (darkening) of the node on T2- and T2*-weighted sequences because of a susceptibility artefact caused by the iron. Metastatic tissue within a node displaces the normal macrophages, thus preventing uptake of contrast agent, and the node continues to remain high in signal intensity. Initial studies indicated a significant increase in sensitivity, with no loss of specificity for the detection of malignant lymph nodes with USPIOs in patients with cervical and endometrial cancer [53]. On a node-by-node basis, the sensitivity increased from 29 % using standard size criteria to 93 % using USPIO criteria. On a patient-by-patient basis, sensitivity increased from 27 % using standard size criteria to 100 % using USPIO criteria. Unfortunately, these data were not confirmed when the agent was trialled in a phase 3 setting and has resulted in a lack of its licensing, so that it is currently unavailable for clinical use.

With the advent of DWI in oncological imaging, this intrinsic contrast mechanism has been

explored for improving detectability of nodes containing metastatic deposits. The European Society of Urogenital Radiology states that diffusion-weighted sequences are optional in staging cervical cancer but are recommended to help evaluate lymph nodes and to detect a residual lesion after chemoradiotherapy [54]; however, there is a paucity of evidence to support this. A number of small single centre studies have reported on the potential of DWI in nodal staging: using the minimum ADC criteria ($\leq 0.881 \times 10^{-3}$ mm^2/s), Liu et al. [55] showed that the sensitivity and specificity for differentiating metastatic from non-metastatic lymph nodes were 95.7 and 96.5 %, respectively. However, in a preliminary study of 26 women with cervical cancer who underwent whole body DWI, the mean ADC value of 16 metastatic nodes was much higher ($0.96 \pm 0.14 \times 10^{-3}$ mm^2/s), although significantly lower than that of benign nodes ($1.39 \pm 0.19 \times 10^{-3}$ mm^2/s, $P = 0.00$). In this study, an ADC threshold value of 1.14×10^{-3} mm^2/s gave a sensitivity of 83 %, specificity 98 % and accuracy 94 % for detecting lymph node involvement [41]. Another retrospective study with 7 positive lymph nodes also suggested significant differences between ADCs of benign vs. malignant nodes, and an ADC threshold value of 0.807×10^{-3} mm^2/s gave a sensitivity, specificity, positive and negative predictive value and accuracy of 100, 98.3, 63.6, 100 and 98.3 %, respectively [56]. However, these studies did not differentiate between small and enlarged nodes, leading to significant reporting bias.

Studies that have included size criteria as well as ADC in their evaluation are more useful. The combination of size and relative ADC values may well be useful in detecting pelvic lymph node metastasis in patients with cervical and uterine cancers (improved sensitivity of 83 % vs. 25 % for the same specificity of 98 % vs. 99 %) with the smallest metastatic lymph node detected being 5 mm in short axis [57]. However, the literature remains conflicting: for example, one study of 680 lymph nodes from 143 patients who underwent radical hysterectomy for uterine cervical cancer gave a specificity and accuracy of mean ADC of 77 and 77 %, compared to 65 and 67 % for short-axis diameter [58], while another prospective study of 18 patients and 340 dissected nodes showed that the differences in the short-axis diameter, the long-axis diameter and the ratio of short- and long-axis diameter on T2-W images between metastatic and non-metastatic nodes and the differences in the ADC values between metastatic and non-metastatic nodes were not significant [59]. A recent small prospective study with good histological correlation, which took into account lymph node size and observer variation, showed that the sensitivity and specificity for detecting lymphatic metastasis by predefined conventional MRI RECIST characteristics were 33 and 83 % on a patient level and 33 and 97 % on regional level, respectively, for observer 1 and 33 and 93 % on a patient level and 25 and 98 % on regional level for observer 2. The kappa value for reproducibility of metastasis detection on regional level was 0.50. The short-axis diameter showed the highest diagnostic accuracy (area under the curve (AUC) = 0.81); ADC did not improve diagnostic accuracy (AUC = 0.83) [60]. No multicenter trial evaluating lymph node status prospectively with ADC as yet exists and is badly needed to address this issue.

35.4 Impact of Optimal Imaging on Clinical Decision Making

35.4.1 Endometrium

Abnormal uterine bleeding in a postmenopausal woman is the most common presenting symptom of endometrial cancer so diagnosis is usually made early, resulting in high survival rates (77 % survival at 5 years) [61]. Following presentation with abnormal uterine bleeding, transvaginal ultrasound is clinically useful in the initial assessment of endometrial cancer and endometrial hyperplasia, with a high sensitivity and specificity of 100 and 79.6 %, respectively [62], identifying those patients with an endometrial thickness of greater than 4 mm who will go on to have an endometrial biopsy. The FIGO classification defines the formal staging of endometrial

cancer based on surgical staging and histopathology. Imaging is an important adjunct to clinical and surgical evaluation in the staging and follow-up of endometrial cancer, and MRI is considered to be the most reliable imaging study in this regard [63]. Management of endometrial cancer is by primary surgery, which consists of total abdominal hysterectomy and bilateral salpingo-oophorectomy. Patients with deep myometrial invasion (>50 %) are treated with adjuvant radiotherapy post-operatively to reduce the risk of recurrence. Vaginal brachytherapy is indicated in cases of endocervical involvement. In patients with inoperable disease or those patients who are unable to undergo surgery due to pre-existing comorbidity, imaging is helpful to define tumour extent for palliative treatment with radiotherapy and chemotherapy [64, 65].

Endometrial cancer spread to the regional lymph nodes is an important prognostic factor [66]. A pelvic and para-aortic node dissection is required for full staging, but a recent large randomised trial (ASTEC) demonstrated no benefit in overall or recurrence-free survival of systematic lymphadenectomy [67]. There is a lack of consensus on which women require a lymphadenectomy and the definition of an adequate lymph node dissection [68]. Current practice is for women at high risk of recurrence (based on imaging and biopsy) to undergo pelvic lymphadenectomy at the time of primary surgery. High-risk tumours demonstrate deep (>50 %) myometrial invasion, cervical involvement or poor differentiation compared to low-risk tumours which are well differentiated, with superficial myometrial invasion, and no enlarged lymph nodes on MRI. Chan et al. [69] demonstrated that a more extensive lymphadenectomy improved the 5-year disease-specific survival rate of patients with intermediate- or high-risk endometrioid uterine cancer. Although, MRI is limited in its ability to differentiate between benign and metastatic lymph nodes of similar size [2, 52], preoperative MRI plays a vital role in identifying the intermediate- or high-risk endometrial cancer cases and thus directing surgery. MRI achieves this by predicting depth of myometrial invasion and cervical stromal involvement and identifying enlarged pelvic and para-aortic lymph nodes and distant spread [2, 63]. FDG PET/CT is useful in the preoperative diagnosis of lymph node metastases, with high accuracy and negative predictive values of 96.8 and 97.2 %, respectively [70], but it is not generally considered sensitive enough to replace lymph node dissection [63].

Tumour extension into the cervix imparts a worse prognosis, and its recognition assists treatment planning [52]. Sagittal images provide a longitudinal view of the uterine body and cervix, although it may be difficult to differentiate endometrial tumour from the high-signal endocervical mucosa [2] (Fig. 35.3). Sagittal images are also useful to assess anterior and posterior tumour extension into the urinary bladder and rectum, respectively. For premenopausal patients with endometrial cancer when fertility-sparing surgery is being considered, MRI aids the correct selection of patients by excluding significant myometrial invasion and ovarian pathology, especially in Lynch syndrome [71].

Morphological MRI is routinely used in post-treatment follow-up of endometrial cancer, and dynamic contrast-enhanced studies are not indicated. The role of DWI is increasingly promising but remains under investigation.

35.4.2 Cervix

Clinical evaluation of cancer of the cervix as per FIGO recommendations is notoriously variable [25, 72], and MRI has become the imaging modality of choice for accurate assessment of the size and extent of the tumour in order to distinguish operable from non-operable disease and determine optimal patient outcome.

Conventional treatment of early-stage cervix-confined disease is with radical hysterectomy in conjunction with pelvic lymph node dissection, while the mainstay of management of advanced disease is chemoradiotherapy. Suitable candidates wishing to preserve their fertility are increasingly considered for trachelectomy (surgical excision of the cervix with vagino-isthmic anastomosis) or extended cone biopsy. Endovaginal MRI is invaluable in preoperative

assessment of these patients. At the other end of the spectrum, MRI can help to identify those patients with bulky stage 1B disease who are at high risk of microscopic nodal disease who may benefit from chemotherapy in addition to radical hysterectomy.

When a fertility-sparing option is sought and where there is vigilant patient selection, radical vaginal trachelectomy (RVT) with pelvic lymph node dissection is similar in efficacy in terms of oncological outcome to radical hysterectomy [73–75]. Taking into account the relative risks of tumour spread and recurrent disease in relation to tumour size, RVT is usually reserved for tumours that are less than 2 cm in diameter and MRI is recommended in the pretreatment size evaluation [25]. Accurate preoperative assessment of the degree of endocervical extension is also mandatory to ensure an adequate clearance at surgery, and most surgeons require 1 cm of tumour-free cervix proximal to the tumour [76, 77]. An adequate volume of residual healthy cervical stroma also lowers the risks of cervical incompetence, infection, premature rupture of membranes and premature delivery in subsequent pregnancies [78]. Extension of tumour to or beyond the internal os will exclude the patient from selection for trachelectomy.

35.5 Recognising Unusual Pathologies

35.5.1 Lymphoma

Patients commonly present with abnormal vaginal blood loss or discharge [79, 80] as well as abdominal pain, but these symptoms are not specific for lymphoma. Because of its stromal rather than epithelial origin, cervical smears are usually negative [81], and histology from deep biopsies is needed to confirm the diagnosis. These tumours are usually diffuse B-cell NHL types and are staged using both the FIGO and also the Ann Arbor classification systems based on findings on the CT scan and bone marrow biopsy [82]. MRI is recommended rather than a CT scan as it is more discerning in differentiating cervical and uterine lymphomas from other entities [79]. MRI demonstrates homogenous signal intensity throughout the myometrium, in an expanded uterus that has lost zonal differentiation on T2-W scans and that enhances homogenously [83–85]. Enhancement is centred on the stroma often sparing the endometrium or cervical mucosa which can help to distinguish lymphoma from the more common endometrial or cervical carcinoma [86]. As with lymphoma at other sites, the prognosis of the patient depends on the stage of the disease, the location and the subtype of lymphoma. Primary cervical lymphoma typically has a good prognosis even with locally advanced disease at presentation and is treated with chemotherapy alone (a fertility-sparing option) or in combination with radiotherapy and/or surgery [87].

35.5.2 Minimal Deviation Adenocarcinoma

First described by Silverberg and Hurst in 1975 [88], minimal deviation adenocarcinoma (MDA), which is also known as adenoma malignum, is a rare form of low-grade mucinous cervical adenocarcinoma that usually presents with watery vaginal discharge or dysfunctional uterine bleeding. It accounts for less than 3 % of cervical adenocarcinomas but a higher incidence has been found in those with Peutz-Jeghers syndrome [89].

Accurate diagnosis of this rare tumour is notoriously difficult but early detection is of paramount importance as optimal treatment in early disease is surgery. Tumours that present later are not amenable to surgery and are treated with chemoradiotherapy to which they are unfortunately relatively insensitive. It is staged using the FIGO system [5], and the mean survival is 5 years for patients with stage 1 disease which drops to 38.1 months with stage 2 disease, 22.8 months with stage 3 disease and 5.4 months with stage 4 disease [90]. There is a high rate

of diagnostic uncertainty in relation to MDA at cervical smear and diagnosis relies on deep cervical biopsies with subsequent antigen detection at immunochemistry.

The imaging modality of choice is MRI and typical findings are that of a multicystic mass with a varying volume of thin solid elements extending from the endocervix to the deep stroma. The solid elements are usually irregular and their presence is associated with invasion and metastases [89]. Alternative findings include simple enlargement of the cervix or fine villous lesions [91]. The cystic elements are usually hypo- or iso-intense to the cervix on T1-weighted imaging and hyperintense on T2-weighted imaging. Both the solid and the cystic elements enhance after contrast administration.

The main differential diagnosis on MR imaging is that of the presence of extensive nabothian cyst (dilated endocervical glands) formation especially if they extend to the deep cervical stroma [92]. The 'tunnel cluster' is a specific type of nabothian cyst that displays multicystic dilatation similar to that seen in minimal deviation adenocarcinoma but without solid elements [93]. Infection with the sexually transmitted diseases Neisseria gonorrhoeae and Chlamydia trachomatis can affect the endocervical glands and can also give MRI appearances similar to MDA, and although these infections can cause vaginal discharge, microbiology should distinguish between MDA and infection. Functional imaging techniques have not been routinely employed to assist discrimination of MDA from other cervical cancer types.

35.5.3 Endometrial Stromal Sarcoma

Endometrial stromal sarcoma is a very rare malignant endometrial mesenchymal tumour, which accounts for only 0.2 % of all malignant uterine neoplasms and approximately 10 % of all uterine sarcomas [94]. The 2003 World Health Classification (WHO) divided endometrial stromal tumours (EST) into a benign entity (endometrial stromal nodule (ESN)), and two malignant entities (endometrial stromal sarcoma (ESS) and undifferentiated endometrial sarcoma (UES)), which have distinct pathological characteristics and prognosis [95, 94]. Endometrial stromal nodules (ESN) are often asymptomatic, being an incidental finding at hysterectomy performed for another reason, and they have an excellent prognosis. The key difference between ESN and the malignant ESTs is the tumour margin. ESN have an expansile, smooth and non-infiltrating margin [96], whereas the malignant ESTs have an irregular and infiltrative margin, which tend to invade into the myometrium to varying degrees [97]. ESS tend to occur in younger patients than UES [97], and they are indolent tumours with a good prognosis (5-year actuarial survival of 98 %, reducing to 89 % at 10 years). In comparison, UES are aggressive tumours with a mean age of onset of 61 years and a poor prognosis with most patients dying within 2 years [96, 97]. Up to 1988, the same staging was used for EST as for endometrial cancers, but a new staging system was developed for uterine sarcomas by FIGO to better reflect the different biological behaviour of these tumours. EST shares the same staging as leiomyosarcomas, with stage I subdivided by size, and no account taken of myometrial invasion [96]. Extrauterine tumour extent at the time of hysterectomy is the major prognostic factor for ESS and UES [95].

Although formal staging is surgical, imaging, particularly MRI, plays an important role in preoperative diagnosis because EST has no specific clinical symptoms or laboratory findings, and particularly in the case of ESS, which occur in younger patients when malignancy is not anticipated [97]. Abnormal uterine bleeding is the commonest presentation of patients with ESS or UES. Treatment consists of hysterectomy and bilateral salpingo-oophorectomy, with or without adjuvant radiotherapy or hormonal treatment [96]. The key MRI findings are of endometrial thickening or a polypoidal mass that usually involves the myometrium extensively, either with a sharply demarcated border or diffusely infiltrative [97]. In a study of 6 patients with ESS and 2 patients with UES, Koyama et al. [97] demonstrated variable MRI findings of these tumours from a polypoidal endometrial

mass to diffuse myometrial thickening. They found that the most important MR imaging feature of ESS was 'worm-like' low T2 signal bands within the area of myometrial invasion, which correlates with the histological findings [97], that are not present if the ESS is confined to the endometrium. Other key MRI features of ESS are continuous tumour extension along the fallopian tubes, tumour surrounding uterine ligaments or ovaries and intratumoural signal voids due to the hypervascular nature of this tumour. In another MRI study of uterine sarcomas, consisting of 3 patients with primary UES and 1 patient with recurrent UES disease, Sahdev et al. demonstrated that UES tends to be an intermediate intensity T1 and T2 endometrial mass, with MRI features that are indistinguishable from endometrial cancer [98]. UES tend to show more of the characteristic MRI findings than ESS, due to their aggressivity [99].

Most ESS and UES enhance more than normal myometrium after contrast administration, in comparison with endometrial cancers that enhance poorly [99], making contrast enhancement a differentiating factor between EST and endometrial cancer. DCE has been shown to be useful in ESS by improving the detection of the tumour margin, intramyometrial nodule extension and myometrial invasion [99]. There is also a paucity of published work on DWI in ESS, although impeded diffusion has been cited in three cases of EST [100, 101].

The differential diagnosis for an ESS includes adenomyosis, leiomyoma and ESN. The typical MRI finding for adenomyosis is extensive low T2 signal in the myometrium and leiomyomas are usually more focal areas of low T2 signal in the myometrium, whereas ESS demonstrate high T2 signal. Both ESS and a leiomyoma can undergo cystic degeneration, resulting in pockets of T2 high signal within the mass, which may cause diagnostic confusion, but leiomyomas almost always have sharply demarcated borders whereas ESS often have an infiltrative margin [97]. DWI, in combination with morphological imaging, may aid differentiation between ESS and degenerated leiomyomas as ADC is generally lower in malignant lesions [101]. However, the large overlap in ADC between uterine sarcomas and ordinary or cellular benign leiomyomas limits clinical utility [101].

Local tumour recurrence occurs in approximately half of patients with ESS, with a median time to recurrence of 3–5 years, but may exceed 20 years. Long-term imaging follow-up is therefore warranted to detect recurrence. Distant metastases are less common [94]. Sahdev et al. [98] found that all 6 patients with local recurrence of their uterine sarcoma, including one patient with recurrence of their UES, had a large heterogeneous T2 signal pelvic mass, which contained whorls of intermediate or low signal intensity and small focal areas of high signal that represented areas of cystic necrosis. DCE and DWI have not been explored for identifying recurrent EST.

35.5.4 Metastases to the Uterus

Metastatic disease to the female genital tract most often involves the ovaries (86.5 % [102]) with endometrial involvement in 3.8 % and cervical involvement in 3.4 % of cases. The commonest tumour to metastasize to the uterus is breast (Fig. 35.6) [103–109] with isolated cervical metastases in some cases [110]. A possible explanation is that the cervix is a small target organ with limited blood supply and one afferent lymphatic drainage system. The fibrous proliferation and inflammatory cellular reaction induced result in an expanded, indurated cervix [111]. It is known that invasive, lobular breast cancers are responsible for >80 % of metastases in gynaecological organs [112]. It is not understood why a different incidence of metastatic disease exists between infiltrating lobular and ductal carcinoma; loss of the adhesion molecule E-cadherin in infiltrating lobular carcinoma but not in ductal carcinoma has been postulated as a possible explanation [113, 114]. In some cases, it can be virtually impossible to discriminate between primary cervical tumours and metastatic lesions from the breast, since functional MRI parameters and reactivity for oestrogen receptors, progesterone receptors and cytokeratin 7 are similar in both cases. Metastatic

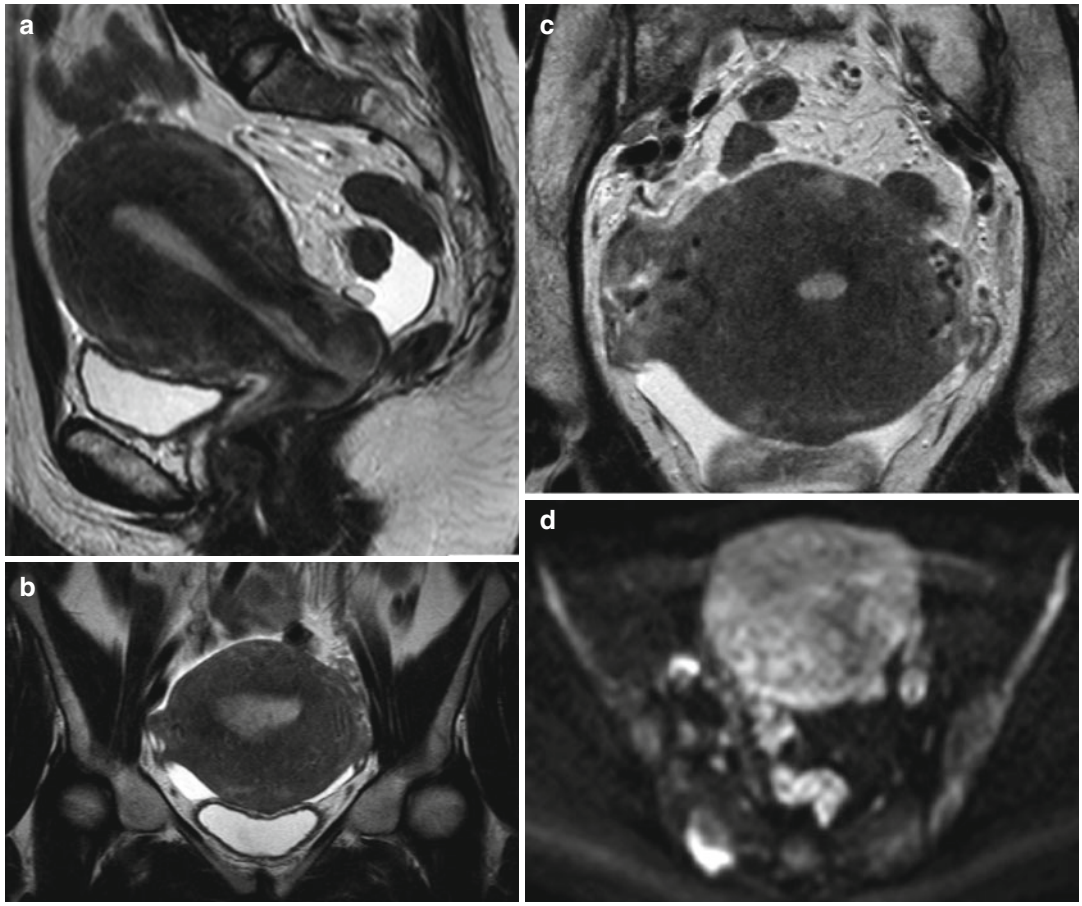

Fig. 35.6 Metachronous uterine metastasis in a 40-year-old woman with history of invasive ductal breast carcinoma: T2-weighted sagittal (**a**), coronal (**b**), and transverse small field of view (**c**) images demonstrate an enlarged uterus, with diffusely abnormal heterogeneous low-signal intensity within the myometrium. There is diffuse high signal within the myometrium on the transverse DWI image (**d**, **b**= 750 smm^{-2}), consistent with tumor infiltration

uterine lesions demand aggressive treatment if they represent the sole site of metastasis. A surgical approach is often preferred; alternatively, taxane-based chemotherapy may be considered. The role of functional imaging in these instances is to confirm absence of other metastatic sites.

35.6 Imaging Disease Response

In conjunction with clinical examination, MR imaging can provide an objective assessment of the effects of surgery or radiotherapy (Fig. 35.7). Serial MR imaging may be used before and after primary radiation therapy to assess tumour response [115] and is increasingly important with the increased use of cytotoxic regimens and newer targeted agents. An increase in signal intensity within the first 2 weeks of treatment is associated with better tumour regression, local control, disease-free survival and overall survival [116–118]. Many studies also have assessed the predictive role of pretreatment tumour enhancement [119–121]. However, although there is clear evidence that increased enhancement after initiation of treatment predicts for favourable therapeutic outcome [118, 120–123], it is difficult to draw conclusions from the literature regarding the predictive role of baseline contrast-enhanced DCE in predicting response. Compared to the literature on DCE,

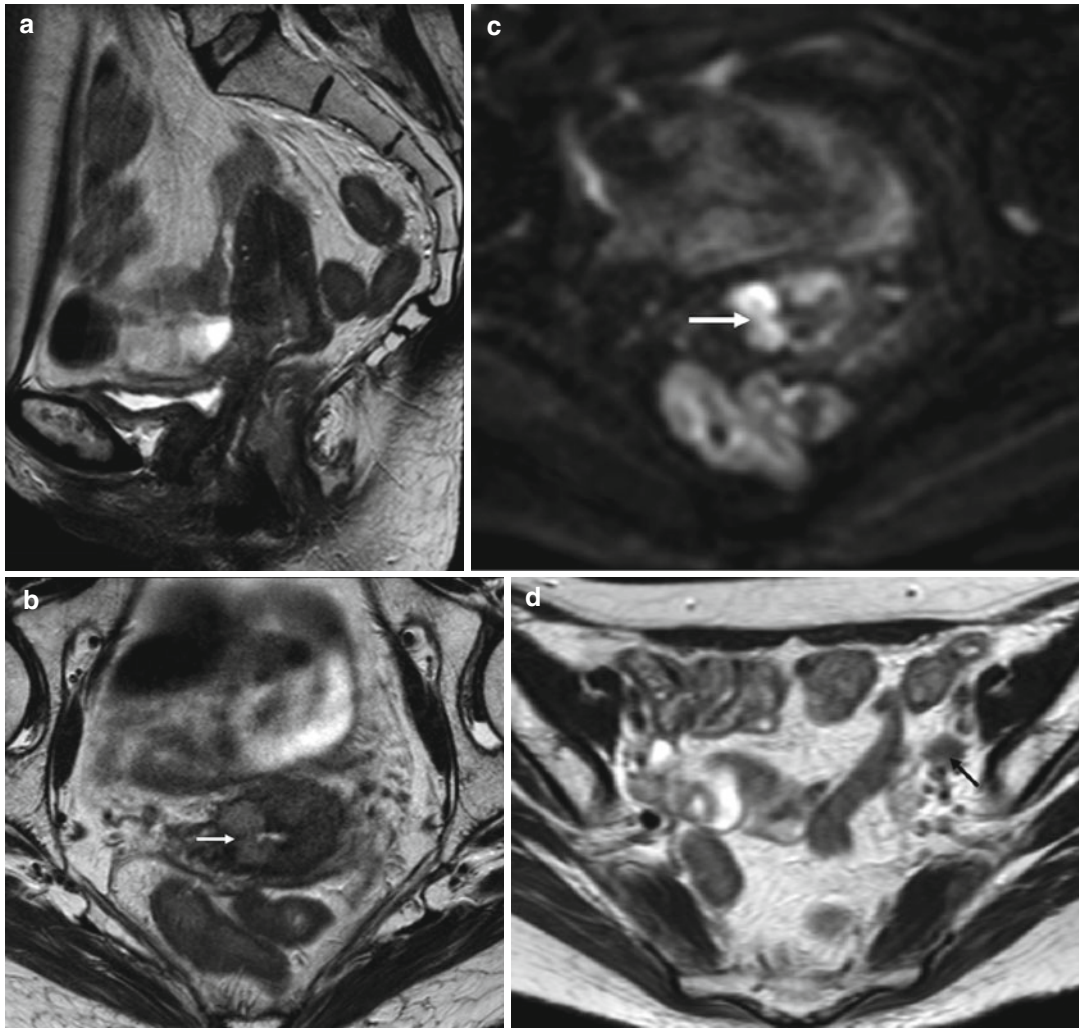

Fig. 35.7 Squamous cell carcinoma of the cervix post-external beam radiotherapy in a 59-year-old female. T2-weighted sagittal (**a**) and transverse (**b**) images demonstrate intermediate signal involving the right lateral side of the cervix (**b**, *arrow*). The residual tumor has impeded diffusion (*arrow*) on the corresponding transverse small field of view DWI (**c**, **b** = 750 smm^{-2}), making it easier to identify than on T2-weighted images. The transverse T1-weighted image (**d**) demonstrates an enlarged left external iliac territory lymph node (*arrow*), which is likely to be involved

the use of ADC in therapeutic monitoring, where extracellular water increases as tumours undergo apoptosis and necrosis, is in its infancy. The mean ADC of cervical cancer is known to increase during and after chemoradiotherapy so that, as with DCE, early alterations in ADC can be used for prediction of early therapeutic response [124]. The demonstration of a significantly lower pretreatment ADC value compared to posttreatment ADC 3 months after completion of chemoradiotherapy (1.0×10^{-3} mm^2/s vs. 1.4×10^{-3} mm^2/s, $P<0.001$) meant that the use of a posttreatment ADC threshold of 1.5×10^{-3} mm^2/s could predict the response to chemoradiation with sensitivity and specificity of 70 and 81.8 %, respectively [124]. In another pilot study of 20 patients, the increase in ADC after 2 weeks of chemoradiotherapy correlated with response as assessed by size reduction at the end of treatment [125].

Unlike the literature on DCE, differences in baseline intratumoural diffusion have also been reported to predict for difference in treatment

response. In a prospective study, Liu et al. [126] observed higher odds of complete response in those with lower baseline ADC values. While complete responders had an average baseline ADC of 0.80×10^{-3} mm^2/s, those with partial response had an average ADC of 0.93×10^{-3} mm^2/s ($P = 0.005$). A negative correlation was found between pretreatment ADCs and percentage size reduction after 2 months of chemoradiation, and percentage ADC change after 1 month correlated positively with percentage size reduction after 2 months of therapy [126].

MRS has also been used for response evaluation to neoadjuvant chemotherapy in cervical cancer prior to radical hysterectomy. The reduction in tumour volume has been associated with reduction in triglyceride levels [51]; however, the technique is not sufficiently robust for routine clinical use.

35.7 Imaging Disease Recurrence

CT and MRI are both used for the detection of recurrent and metastatic disease. CT has a diagnostic accuracy of 92 % in the detection of a relapse of uterine cancer [127]. Following surgery or effective chemoradiation to the pelvis, where there is often postsurgical or posttreatment fibrosis, the identification of small-volume disease recurrence may be difficult because CT and ultrasound have limited ability to differentiate between fibrosis and tumour. The better differentiation between the tumour and posttreatment fibrotic tissue on MRI than CT makes MRI the preferred modality to detect recurrence posttreatment [2]. Without the use of a dynamic contrast-enhanced acquisition, the use of contrast agents in detecting recurrent disease can be disappointing unless there is a specific remit to identify treatment complications (e.g. fistula formation), when post-contrast images are useful [128]. Initial studies using DCE to detect recurrence in previously treated cervical cancer indicated that the accuracy of depicting recurrent tumour on dynamic images (82 %) was superior to that of pre- and post-contrast T1-weighted images and T2-weighted images (64, 68 and 64 %, respectively). The dynamic nature of the DCE data acquisition is crucially important diagnostically as these images provide better contrast between the recurrent tumour and pelvic fat than the T2-weighted or post-contrast T1-weighted images [129].

The value of pretreatment perfusion data as a prognostic indicator for recurrence also has been explored—a study of 88 patients treated with radiotherapy who underwent serial DCE before RT, at 20–22 Gy, and at 45–50 Gy, showed that local recurrence predominated in the group who had both a low mean haemoglobin (<11.2 g/dL) and low perfusion (lowest 10th percentile of signal intensity <2.0 at 20–22 Gy), with a 5-year local control rate of 60 % compared to 90 % for all other groups ($p = .001$) and a disease-specific survival rate of 41 % compared to 72 % ($p = .008$), respectively. In the group of patients with both high mean haemoglobin and high perfusion, the 5-year local control rate and disease-specific survival rate were 100 % and 78 %, respectively [130]. Furthermore, the addition of MRI parameters (perfusion, volume) to clinical prognostic factors increased sensitivity and specificity of clinical prognostic factors from 71 and 51 %, respectively, to 100 and 71 %, respectively, for predicting recurrence and from 79 and 54 %, respectively, to 93 and 60 %, respectively, for predicting death [120]. Data from another study, however, contradicts this, where tumours with high enhancing fraction had a significantly poorer Probability of disease-free survival than those with low enhancing fraction [131].

Data on use of ADC to detect disease recurrence is sparse—in a series of 112 patients with cervical cancer published recently, 18 had recurrent tumours and all these were recognised on the ADC maps [132]. There are no published papers on the value of DW MRI in detection of tumour recurrence in endometrial cancer. This is because of difficulties in obtaining histopathological correlation in these cases where further radiotherapy or chemotherapy or a combination is the standard of care. In our experience, DW MRI is very useful in detection of localised tumour recurrence within the pelvis as well as detection of disseminated peritoneal recurrence.

Areas of tumour recurrence appear bright on DW images and demonstrate restricted diffusion on the ADC maps.

Conclusion

Functional MRI has found its way into the clinical assessment of patients with gynaecological malignancy. A variety of techniques are available and their readouts provide a quantitative means of assessing disease. Of these, DCE and DWI are used most routinely. DCE techniques require administration of extrinsic contrast agents, whereas DWI exploits intrinsic contrast mechanisms. The latter is often preferred particularly in the response assessment setting as it is easier to implement, quicker and can be used to cover anything from a dedicated region of interest to the whole body. However, quantifiable parameters can vary significantly in their reproducibility, and standardised methods of patient preparation and image acquisition are needed to ensure that the technical quality of the information is sufficient to yield reliable quantitative data. Methods of analysis also need consensus and standardisation before interpretation of quantitative parameters can be used in multicenter trials or can be applied universally.

References

1. Allisy-Roberts PJ, Williams JR. Farr's physics for medical imaging. 2nd ed. Edinburgh: Saunders Ltd; 2007.
2. Whitten CR, DeSouza NM. Magnetic resonance imaging of uterine malignancies. Top Magn Reson Imaging. 2006;17(6):365–77.
3. Tofts PS. Modeling tracer kinetics in dynamic Gd-DTPA MR imaging. J Magn Reson Imaging. 1997;7(1):91–101.
4. Hallac RR, et al. Oxygenation in cervical cancer and normal uterine cervix assessed using blood oxygenation level-dependent (BOLD) MRI at 3T. NMR Biomed. 2012;25(12):1321–30.
5. Pecorelli S. Revised FIGO staging for carcinoma of the vulva, cervix, and endometrium. Int J Gynaecol Obstet. 2009;105(2):103–4.
6. Frei KA, et al. Prediction of deep myometrial invasion in patients with endometrial cancer: clinical utility of contrast-enhanced MR imaging-a meta-analysis and Bayesian analysis. Radiology. 2000;216(2):444–9.
7. Kinkel K, et al. Radiologic staging in patients with endometrial cancer: a meta-analysis. Radiology. 1999;212(3):711–8.
8. Joja I, et al. Endometrial carcinoma: dynamic MRI with turbo-FLASH technique. J Comput Assist Tomogr. 1996;20(6):878–87.
9. Nasi F, et al. MRI evaluation of myometrial invasion by endometrial carcinoma. Comparison between fast-spin-echo T2w and coronal-FMPSPGR Gadolinium-Dota-enhanced sequences. Radiol Med. 2005;110(3):199–210.
10. Rechichi G, et al. Myometrial invasion in endometrial cancer: diagnostic performance of diffusion-weighted MR imaging at 1.5-T. Eur Radiol. 2010;20(3):754–62.
11. Shen SH, et al. Diffusion-weighted single-shot echo-planar imaging with parallel technique in assessment of endometrial cancer. AJR Am J Roentgenol. 2008;190(2):481–8.
12. Wang J, et al. The value of the apparent diffusion coefficient in differentiating stage IA endometrial carcinoma from normal endometrium and benign diseases of the endometrium: initial study at 3-T magnetic resonance scanner. J Comput Assist Tomogr. 2010;34(3):332–7.
13. Fujii S, et al. Diagnostic accuracy of the apparent diffusion coefficient in differentiating benign from malignant uterine endometrial cavity lesions: initial results. Eur Radiol. 2008;18(2):384–9.
14. Rechichi G, et al. Endometrial cancer: correlation of apparent diffusion coefficient with tumor grade, depth of myometrial invasion, and presence of lymph node metastases. AJR Am J Roentgenol. 2011;197(1):256–62.
15. Levy A, et al. Interest of diffusion-weighted echo-planar MR imaging and apparent diffusion coefficient mapping in gynecological malignancies: a review. J Magn Reson Imaging. 2011;33(5):1020–7.
16. Kim SH, et al. Preoperative staging of uterine cervical carcinoma: comparison of CT and MRI in 99 patients. J Comput Assist Tomogr. 1993;17(4):633–40.
17. Ozsarlak O, et al. The correlation of preoperative CT, MR imaging, and clinical staging (FIGO) with histopathology findings in primary cervical carcinoma. Eur Radiol. 2003;13(10):2338–45.
18. Sala E, et al. MRI of malignant neoplasms of the uterine corpus and cervix. AJR Am J Roentgenol. 2007; 188(6):1577–87.
19. Soutter WP, et al. Pretreatment tumour volume measurement on high-resolution magnetic resonance imaging as a predictor of survival in cervical cancer. BJOG. 2004;111(7):741–7.
20. Mitchell DG, et al. Early invasive cervical cancer: MRI and CT predictors of lymphatic metastases in the ACRIN 6651/GOG 183 intergroup study. Gynecol Oncol. 2009;112(1):95–103.
21. Burghardt E, et al. Magnetic resonance imaging in cervical cancer: a basis for objective classification. Gynecol Oncol. 1989;33(1):61–7.
22. Greco A, et al. Staging of carcinoma of the uterine cervix: MRI-surgical correlation. Clin Radiol. 1989; 40(4):401–5.

23. Hricak H, et al. Invasive cervical carcinoma: comparison of MR imaging and surgical findings. Radiology. 1988;166(3):623–31.
24. Lien HH, et al. Clinical stage I carcinoma of the cervix. Value of MR imaging in determining invasion into the parametrium. Acta Radiol. 1993;34(2):130–2.
25. Subak LL, et al. Cervical carcinoma: computed tomography and magnetic resonance imaging for preoperative staging. Obstet Gynecol. 1995;86(1):43–50.
26. Wagenaar HC, et al. Tumor diameter and volume assessed by magnetic resonance imaging in the prediction of outcome for invasive cervical cancer. Gynecol Oncol. 2001;82(3):474–82.
27. deSouza NM, et al. Magnetic resonance imaging of the primary site in stage I cervical carcinoma: a comparison of endovaginal coil with external phased array coil techniques at 0.5T. J Magn Reson Imaging. 2000;12(6):1020–6.
28. Ebner F, et al. Magnetic resonance imaging in cervical carcinoma: diagnosis, staging, and follow-up. Magn Reson Q. 1994;10(1):22–42.
29. Fischetti SG, et al. Carcinoma of the uterine cervical canal. Staging and biometric assessment with magnetic resonance. Radiol Med. 1994;88(4):445–52.
30. Hawnaur JM, et al. Staging, volume estimation and assessment of nodal status in carcinoma of the cervix: comparison of magnetic resonance imaging with surgical findings. Clin Radiol. 1994;49(7):443–52.
31. Narayan K, et al. Relation between FIGO stage, primary tumor volume, and presence of lymph node metastases in cervical cancer patients referred for radiotherapy. Int J Gynecol Cancer. 2003;13(5):657–63.
32. Seki H, et al. Stromal invasion by carcinoma of the cervix: assessment with dynamic MR imaging. AJR Am J Roentgenol. 1997;168(6):1579–85.
33. Hawighorst H, et al. Evaluation of angiogenesis and perfusion of bone marrow lesions: role of semiquantitative and quantitative dynamic MRI. J Magn Reson Imaging. 1999;10(3):286–94.
34. Lyng H, et al. Oxygen tension and vascular density in human cervix carcinoma. Br J Cancer. 1996;74(10):1559–63.
35. Cooper RA, et al. Changes in oxygenation during radiotherapy in carcinoma of the cervix. Int J Radiat Oncol Biol Phys. 1999;45(1):119–26.
36. Postema S, et al. Cervical carcinoma: can dynamic contrast-enhanced MR imaging help predict tumor aggressiveness? Radiology. 1999;210(1):217–20.
37. deSouza NM, et al. Cervical cancer: value of an endovaginal coil magnetic resonance imaging technique in detecting small volume disease and assessing parametrial extension. Gynecol Oncol. 2006;102(1):80–5.
38. deSouza NM, et al. Value of magnetic resonance imaging with an endovaginal receiver coil in the pre-operative assessment of stage I and IIa cervical neoplasia. Br J Obstet Gynaecol. 1998;105(5):500–7.
39. deSouza NM, et al. High-resolution MR imaging of stage I cervical neoplasia with a dedicated transvaginal coil: MR features and correlation of imaging and pathologic findings. AJR Am J Roentgenol. 1996;166(3):553–9.
40. Charles-Edwards EM, et al. Diffusion-weighted imaging in cervical cancer with an endovaginal technique: potential value for improving tumor detection in stage Ia and Ib1 disease. Radiology. 2008;249(2):541–50.
41. Chen YB, et al. Staging of uterine cervical carcinoma: whole-body diffusion-weighted magnetic resonance imaging. Abdom Imaging. 2011;36(5):619–26.
42. Hoogendam JP, et al. The influence of the b-value combination on apparent diffusion coefficient based differentiation between malignant and benign tissue in cervical cancer. J Magn Reson Imaging. 2010;32(2):376–82.
43. Kilickesmez O, et al. Quantitative diffusion-weighted magnetic resonance imaging of normal and diseased uterine zones. Acta Radiol. 2009;50(3):340–7.
44. Payne GS, et al. Evaluation of magnetic resonance diffusion and spectroscopy measurements as predictive biomarkers in stage 1 cervical cancer. Gynecol Oncol. 2010;116(2):246–52.
45. Xue HD, et al. Clinical application of body diffusion weighted MR imaging in the diagnosis and preoperative N staging of cervical cancer. Chin Med Sci J. 2008;23(3):133–7.
46. Liu Y, et al. Diffusion-weighted magnetic resonance imaging of uterine cervical cancer. J Comput Assist Tomogr. 2009;33(6):858–62.
47. Downey K, et al. Relationship between imaging biomarkers of stage I cervical cancer and poor-prognosis histologic features: quantitative histogram analysis of diffusion-weighted MR images. AJR Am J Roentgenol. 2013;200(2):314–20.
48. Hricak H, et al. Role of imaging in pretreatment evaluation of early invasive cervical cancer: results of the intergroup study American College of Radiology Imaging Network 6651-Gynecologic Oncology Group 183. J Clin Oncol. 2005;23(36):9329–37.
49. Yamashita Y, et al. Carcinoma of the cervix: dynamic MR imaging. Radiology. 1992;182(3):643–8.
50. Mahon MM, et al. (1)H magnetic resonance spectroscopy of preinvasive and invasive cervical cancer: in vivo-ex vivo profiles and effect of tumor load. J Magn Reson Imaging. 2004;19(3):356–64.
51. Booth SJ, et al. In vivo magnetic resonance spectroscopy of gynaecological tumours at 3.0 Tesla. BJOG. 2009;116(2):300–3.
52. Manfredi R, et al. Local-regional staging of endometrial carcinoma: role of MR imaging in surgical planning. Radiology. 2004;231(2):372–8.
53. Rockall AG, et al. Diagnostic performance of nanoparticle-enhanced magnetic resonance imaging in the diagnosis of lymph node metastases in patients with endometrial and cervical cancer. J Clin Oncol. 2005;23(12):2813–21.
54. Balleyguier C, et al. Staging of uterine cervical cancer with MRI: guidelines of the European Society of Urogenital Radiology. Eur Radiol. 2011;21(5):1102–10.
55. Liu Y, et al. Differentiation of metastatic from non-metastatic lymph nodes in patients with uterine

cervical cancer using diffusion-weighted imaging. Gynecol Oncol. 2011;122(1):19–24.
56. Rechichi G, et al. ADC maps in the prediction of pelvic lymph nodal metastatic regions in endometrial cancer. Eur Radiol. 2013;23(1):65–74.
57. Lin G, et al. Detection of lymph node metastasis in cervical and uterine cancers by diffusion-weighted magnetic resonance imaging at 3T. J Magn Reson Imaging. 2008;28(1):128–35.
58. Kim MH, et al. Diagnosis of lymph node metastasis in uterine cervical cancer: usefulness of computer-aided diagnosis with comprehensive evaluation of MR images and clinical findings. Acta Radiol. 2011;52(10):1175–83.
59. Nakai G, et al. Detection and evaluation of pelvic lymph nodes in patients with gynecologic malignancies using body diffusion-weighted magnetic resonance imaging. J Comput Assist Tomogr. 2008;32(5):764–8.
60. Klerkx WM, et al. The value of 3.0Tesla diffusion-weighted MRI for pelvic nodal staging in patients with early stage cervical cancer. Eur J Cancer. 2012;48(18):3414–21.
61. Office for National Statistics. Cancer survival in England: patients diagnosed 2005–2009 and followed up to 2010. England: Office for National Statistics; 2011.
62. Minagawa Y, et al. Transvaginal ultrasonography and endometrial cytology as a diagnostic schema for endometrial cancer. Gynecol Obstet Invest. 2005; 59(3):149–54.
63. Patel S, et al. Imaging of endometrial and cervical cancer. Insights Imaging. 2010;1(5–6):309–28.
64. Husband J, Reznek RH, editors. Imaging in oncology, vol. 1. Oxford: Oxford Press; 1998.
65. Husband JE, Reznek RH. Imaging in oncology, vol. 1. London/Boca Raton: Taylor & Francis; 2004.
66. Mariani A, et al. Significance of pathologic patterns of pelvic lymph node metastases in endometrial cancer. Gynecol Oncol. 2001;80(2):113–20.
67. Kitchener H, et al. Efficacy of systematic pelvic lymphadenectomy in endometrial cancer (MRC ASTEC trial): a randomised study. Lancet. 2009;373(9658):125–36.
68. Lewin SN. Revised FIGO staging system for endometrial cancer. Clin Obstet Gynecol. 2011;54(2):215–8.
69. Chan JK, et al. Therapeutic role of lymph node resection in endometrioid corpus cancer: a study of 12,333 patients. Cancer. 2006;107(8):1823–30.
70. Signorelli M, et al. Role of the integrated FDG PET/CT in the surgical management of patients with high risk clinical early stage endometrial cancer: detection of pelvic nodal metastases. Gynecol Oncol. 2009; 115(2):231–5.
71. Wright JD, et al. Contemporary management of endometrial cancer. Lancet. 2012;379(9823):1352–60.
72. Togashi K, et al. Cervical cancer. J Magn Reson Imaging. 1998;8(2):391–7.
73. Beiner ME, et al. Radical vaginal trachelectomy vs. radical hysterectomy for small early stage cervical cancer: a matched case–control study. Gynecol Oncol. 2008;110(2):168–71.
74. Covens A, et al. Is radical trachelectomy a safe alternative to radical hysterectomy for patients with stage IA-B carcinoma of the cervix? Cancer. 1999;86(11):2273–9.
75. Marchiole P, et al. Oncological safety of laparoscopic-assisted vaginal radical trachelectomy (LARVT or Dargent's operation): a comparative study with laparoscopic-assisted vaginal radical hysterectomy (LARVH). Gynecol Oncol. 2007;106(1):132–41.
76. Milliken DA, Shepherd JH. Fertility preserving surgery for carcinoma of the cervix. Curr Opin Oncol. 2008;20(5):575–80.
77. Shepherd JH. Cervical cancer. Best Pract Res Clin Obstet Gynaecol. 2012;26(3):293–309.
78. Rob L, et al. Fertility-sparing surgery in patients with cervical cancer. Lancet Oncol. 2011;12(2):192–200.
79. Frey NV, et al. Primary lymphomas of the cervix and uterus: the University of Pennsylvania's experience and a review of the literature. Leuk Lymphoma. 2006;47(9):1894–901.
80. Yamamoto T, et al. Intravascular large B-cell lymphoma of the uterus: a case with favorable clinical outcome. Int J Surg Pathol. 2011;19(5):672–6.
81. Chan JK, et al. Clinicopathologic features of six cases of primary cervical lymphoma. Am J Obstet Gynecol. 2005;193(3 Pt 1):866–72.
82. Heeren JH, et al. Primary extranodal marginal zone B-cell lymphoma of the female genital tract: a case report and literature review. Int J Gynecol Pathol. 2008;27(2):243–6.
83. Dang HT, et al. Primary lymphoma of the cervix: MRI findings with gadolinium. Magn Reson Imaging. 1991;9(6):941–4.
84. Kawakami S, et al. MR appearance of malignant lymphoma of the uterus. J Comput Assist Tomogr. 1995;19(2):238–42.
85. Marin C, et al. Magnetic resonance imaging of primary lymphoma of the cervix. Eur Radiol. 2002;12(6):1541–5.
86. Muntz HG, et al. Stage IE primary malignant lymphomas of the uterine cervix. Cancer. 1991;68(9): 2023–32.
87. Okamoto Y, et al. MR imaging of the uterine cervix: imaging-pathologic correlation. Radiographics. 2003;23(2):425–45; quiz 534–425.
88. Silverberg SG, Hurt WG. Minimal deviation adenocarcinoma ("adenoma malignum") of the cervix: a reappraisal. Am J Obstet Gynecol. 1975;121(7):971–5.
89. Park SB, et al. Adenoma malignum of the uterine cervix: imaging features with clinicopathologic correlation. Acta Radiol. 2013;54(1):113–20.
90. Li G, et al. Minimal deviation adenocarcinoma of the uterine cervix. Int J Gynaecol Obstet. 2010; 110(2):89–92.
91. Itoh K, et al. A comparative analysis of cross sectional imaging techniques in minimal deviation adenocarcinoma of the uterine cervix. BJOG. 2000; 107(9):1158–63.
92. Clement PB, Young RH. Deep nabothian cysts of the uterine cervix. A possible source of confusion with

minimal-deviation adenocarcinoma (adenoma malignum). Int J Gynecol Pathol. 1989;8(4):340–8.
93. Sugiyama K, Takehara Y. MR findings of pseudoneoplastic lesions in the uterine cervix mimicking adenoma malignum. Br J Radiol. 2007;80(959):878–83.
94. Tavassoli FA, Devilee P. Pathology and genetics:tumours of the breast and female genital organs. World Health Organisation classification of tumours. Lyon: IARC Press; 2003.
95. Evans HL. Endometrial stromal sarcoma and poorly differentiated endometrial sarcoma. Cancer. 1982; 50(10):2170–82.
96. D'Angelo E, Prat J. Uterine sarcomas: a review. Gynecol Oncol. 2010;116(1):131–9.
97. Koyama T, et al. MR imaging of endometrial stromal sarcoma: correlation with pathologic findings. AJR Am J Roentgenol. 1999;173(3):767–72.
98. Sahdev A, et al. MR imaging of uterine sarcomas. AJR Am J Roentgenol. 2001;177(6):1307–11.
99. Ueda M, et al. MR imaging findings of uterine endometrial stromal sarcoma: differentiation from endometrial carcinoma. Eur Radiol. 2001;11(1):28–33.
100. La Fianza A, et al. Magnetic resonance appearance of endometrial sarcoma: report of a case with unusual findings. Magn Reson Imaging. 1999;17(4):637–40.
101. Tamai K, et al. The utility of diffusion-weighted MR imaging for differentiating uterine sarcomas from benign leiomyomas. Eur Radiol. 2008;18(4):723–30.
102. Mazur MT, et al. Metastases to the female genital tract. Analysis of 325 cases. Cancer. 1984;53(9):1978–84.
103. Haji BE, et al. Cytomorphological features of metastatic mammary lobular carcinoma in cervicovaginal smears: report of a case and review of literature. Cytopathology. 2005;16(1):42–8.
104. Hepp HH, et al. Breast cancer metastatic to the uterine cervix: analysis of a rare event. Cancer Invest. 1999;17(7):468–73.
105. Kennebeck CH, Alagoz T. Signet ring breast carcinoma metastases limited to the endometrium and cervix. Gynecol Oncol. 1998;71(3):461–4.
106. Mousavi A, Karimi Zarchi M. Isolated cervical metastasis of breast cancer: a case report and literature review. J Low Genit Tract Dis. 2007;11(4):276–8.
107. Perisic D, et al. Metastasis of lobular breast carcinoma to the cervix. J Obstet Gynaecol Res. 2007; 33(4):578–80.
108. Piura B, et al. Abnormal uterine bleeding as a presenting sign of metastases to the uterine corpus, cervix and vagina in a breast cancer patient on Tamoxifen therapy. Eur J Obstet Gynecol Reprod Biol. 1999;83(1):57–61.
109. Yazigi R, et al. Breast cancer metastasizing to the uterine cervix. Cancer. 1988;61(12):2558–60.
110. Way S. Carcinoma metastatic in the cervix. Gynecol Oncol. 1980;9(3):298–302.
111. Bryson CA, et al. Breast cancer metastasising to the uterine cervix. Ulster Med J. 1999;68(1):30–2.
112. Lamovec J, Bracko M. Metastatic pattern of infiltrating lobular carcinoma of the breast: an autopsy study. J Surg Oncol. 1991;48(1):28–33.
113. Moll R, et al. Differential loss of E-cadherin expression in infiltrating ductal and lobular breast carcinomas. Am J Pathol. 1993;143(6):1731–42.
114. Sastre-Garau X, et al. Infiltrating lobular carcinoma of the breast. Clinicopathologic analysis of 975 cases with reference to data on conservative therapy and metastatic patterns. Cancer. 1996;77(1):113–20.
115. Akin O, et al. Imaging of uterine cancer. Radiol Clin North Am. 2007;45(1):167–82.
116. Semple SI, et al. A combined pharmacokinetic and radiologic assessment of dynamic contrast-enhanced magnetic resonance imaging predicts response to chemoradiation in locally advanced cervical cancer. Int J Radiat Oncol Biol Phys. 2009;75(2):611–7.
117. Takayama Y, et al. Prediction of early response to radiotherapy of uterine carcinoma with dynamic contrast-enhanced MR imaging using pixel analysis of MR perfusion imaging. Magn Reson Imaging. 2009;27(3):370–6.
118. Zahra MA, et al. Semiquantitative and quantitative dynamic contrast-enhanced magnetic resonance imaging measurements predict radiation response in cervix cancer. Int J Radiat Oncol Biol Phys. 2009;74(3):766–73.
119. Mannelli L, et al. Evaluation of nonenhancing tumor fraction assessed by dynamic contrast-enhanced MRI subtraction as a predictor of decrease in tumor volume in response to chemoradiotherapy in advanced cervical cancer. AJR Am J Roentgenol. 2010;195(2):524–7.
120. Mayr NA, et al. Ultra-early predictive assay for treatment failure using functional magnetic resonance imaging and clinical prognostic parameters in cervical cancer. Cancer. 2010;116(4):903–12.
121. Yuh WT, et al. Predicting control of primary tumor and survival by DCE MRI during early therapy in cervical cancer. Invest Radiol. 2009;44(6):343–50.
122. Gong QY, et al. Contrast enhanced dynamic MRI of cervical carcinoma during radiotherapy: early prediction of tumour regression rate. Br J Radiol. 1999;72(864):1177–84.
123. Mayr NA, et al. Longitudinal changes in tumor perfusion pattern during the radiation therapy course and its clinical impact in cervical cancer. Int J Radiat Oncol Biol Phys. 2010;77(2):502–8.
124. Chen J, et al. The utility of diffusion-weighted MR imaging in cervical cancer. Eur J Radiol. 2010; 74(3):e101–6.
125. Harry VN, et al. Diffusion-weighted magnetic resonance imaging in the early detection of response to chemoradiation in cervical cancer. Gynecol Oncol. 2008;111(2):213–20.
126. Liu Y, et al. Diffusion-weighted imaging in predicting and monitoring the response of uterine cervical

cancer to combined chemoradiation. Clin Radiol. 2009;64(11):1067–74.
127. Franchi M, et al. Clinical value of computerized tomography (CT) in assessment of recurrent uterine cancers. Gynecol Oncol. 1989;35(1):31–7.
128. Hricak H, et al. Irradiation of the cervix uteri: value of unenhanced and contrast-enhanced MR imaging. Radiology. 1993;189(2):381–8.
129. Yamashita Y, et al. Dynamic MR imaging of recurrent postoperative cervical cancer. J Magn Reson Imaging. 1996;6(1):167–71.
130. Mayr NA, et al. Synergistic effects of hemoglobin and tumor perfusion on tumor control and survival in cervical cancer. Int J Radiat Oncol Biol Phys. 2009;74(5):1513–21.
131. Donaldson SB, et al. Enhancing fraction measured using dynamic contrast-enhanced MRI predicts disease-free survival in patients with carcinoma of the cervix. Br J Cancer. 2010;102(1):23–6.
132. Kuang F, et al. The value of apparent diffusion coefficient in the assessment of cervical cancer. Eur Radiol. 2012.